Available online at www.sciencedirect.com
ScienceDirect
Journal of the Mechanics and Physics of Solids 56 (2008) 839–857
JOURNAL OF THE MECHANICS AND PHYSICS OF SOLIDS
www.elsevier.com/locate/jmps

# The stress concentration near a rigid line inclusion in a prestressed, elastic material. Part II. Implications on shear band nucleation, growth and energy release rate

Davide Bigoni*, Francesco Dal Corso, Massimiliano Gei

*Department of Mechanical and Structural Engineering, University of Trento, via Mesiano 77, I-38050 Trento, Italy*

Received 30 March 2007; received in revised form 30 June 2007; accepted 3 July 2007

**Abstract**

The full-field and asymptotic solutions derived in Part I of this article (for a lamellar rigid inclusion, embedded in a uniformly prestressed, incompressible and orthotropic elastic sheet, subject to a far-field deformation increment) are employed to analyse shear band formation, as promoted by the near-tip stress singularity. Since these solutions involve the prestress as a parameter, stress and deformation fields can be investigated near the boundary of ellipticity loss (but still within the elliptic range). In the vicinity of this boundary, the incremental stress and displacement fields evidence localized deformations with patterns organized into shear bands, evidencing inclinations corresponding to those predicted at ellipticity loss. These localized deformation patterns are shown to explain experimental results on highly deformed soft materials containing thin, stiff inclusions. Finally, the incremental energy release rate and incremental *J*-integral are derived, related to a reduction (or growth) of the stiffener. It is shown that this is always positive (or negative), but tends to zero approaching the Ellipticity boundary, which implies that reduction of the lamellar inclusion dies out and, simultaneously, shear bands develop.


*Keywords:* Anticrack; Residual stress; Localized deformation; *J*-integral

## 1. Introduction

The near-tip asymptotic solution (involving both Mode I and Mode II loading) and the full-field Mode I solution for a rigid lamellar inclusion (a stiffener) embedded in an infinite, uniformly prestressed and prestrained, incompressible, elastic material, obtained in Part I of the present article, is employed to investigate shear band nucleation and growth. In particular, the solutions, valid within the elliptic range, can

*Corresponding author. Tel.: +39 0461 882507; fax: +39 0461 882599.
*E-mail addresses:* bigoni@ing.unitn.it (D. Bigoni), francesco.dalcorso@ing.unitn.it (F. Dal Corso), mgei@ing.unitn.it (M. Gei).
*URL:* http://www.ing.unitn.it/~bigoni/ (D. Bigoni).

0022-5096/$ - see front matter © 2007 Elsevier Ltd. All rights reserved.
doi:10.1016/j.jmps.2007.07.003

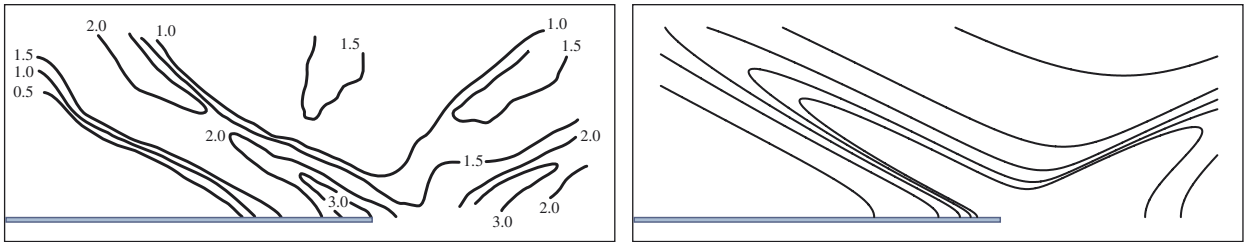


Fig. 1. Deformation near a thin and stiff inclusion: experimental results, deformation map in a Cu matrix near a W platelet (adapted from Öztürk et al., 1991), left, versus analytical solution for a $J_2$-material, prestrained until close to the boundary of ellipticity loss ($\varepsilon = 0.675$ and $N = 0.4$), right.

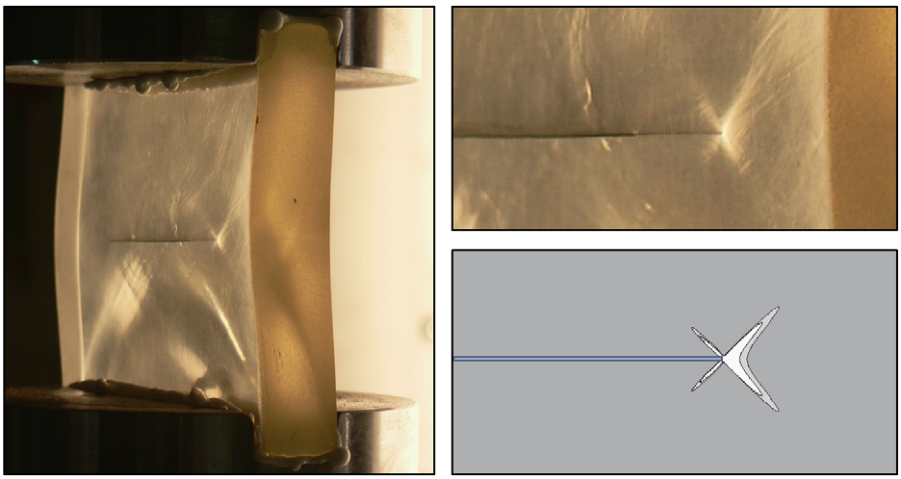

Fig. 2. 100 mm×100 mm×18 mm two-component epoxy resin sample (S3, see Appendix A of Part I of this article) containing a 44 mm×18 mm×0.3 mm aluminum platelet loaded uniaxially in vertical compression (photo taken at the University of Trento in bright light with a Panasonic DMC-FZ5 digital camera at a 50 MPa of compressive stress). The material exhibited a ductile behaviour and suffered an out-of-plane buckling. Light reflection evidences strain localization at the end of the platelet (clearly visible in the detail on the right, upper part). Note the similarity with the analytical solution also reported (right, lower part, obtained for a highly anisotropic material, $\xi = 0.015$, without prestress, $k = 0$, near the boundary of ellipticity loss).

be exploited until near the boundary of ellipticity loss[1] in a way similar to that pawed by Bigoni and Capuani (2002, 2005), thus revealing the emergence of localized deformation patterns.

Shear bands are shown (in Section 2): (i) to be strongly promoted by the near-tip singularity; (ii) to *emanate radially* from the tip of the stiffener; (iii) to have an inclination independent of the perturbing agent; (iv) to form patterns sharing a strict similarity (results obtained with our solution are shown in Figs.1, right, and 2, right, lower part) with those experimentally investigated:

- by Öztürk et al. (1991) in a ductile Cu matrix containing stiff W platelets, see Fig. 1, left;
- by us on a 18 mm thick, 100 mm×100 mm two-component epoxy resin square plate (sample S3 described in Appendix A of Part I of this article) containing a 44 mm×18 mm×0.3 mm aluminum platelet and subject to uniaxial in-plane compression orthogonal to the long edge of the platelet, see Fig. 2, left and right (upper part).

[1]For the problem of a crack prestressed parallel to the free surfaces analysed by Radi et al. (2002), the surface instability occurring at crack flanks prevents (with the exception of the EI/P boundary for $k>0$) the possibility of approaching the boundary of ellipticity loss.

The solution developed in Part I of this paper has been obtained under the assumption of uniform prestress, a situation which cannot obviously be obtained through straining of a sample made of a homogeneous material containing a rigid inclusion (although it could result from a constrained transformation strain), as it occurs in the case of the above-mentioned experiments. However, the similarity between incremental fields near the Elliptic boundary and near-failure strain concentration in the experiments is a fact, corroborated also by numerical tests (performed with Abaqus/Standard Ver. 6.5-1 using a $J_2$-flow theory and a deformation theory material, not reported for conciseness). The explanation for this is that the incremental deformation found near the elliptic boundary in a homogeneously prestressed material is a sort of 'ultimate deformation mode', sweeping the previously accumulated strain and dominating the near-failure fields. Something similar is occurring for perfectly plastic solids, where slip line solutions, obtained without consideration of the previous stress/strain evolution, are in pretty close agreement with shear bands visible in experiments.

Analogously to the akin crack problem (Rice, 1968), it is possible to analyse the energy release rate involved with a growth of the stiffener. This problem has never been considered (even for linear isotropic elasticity without prestress) and can be more effectively understood in relation to a *reduction* than to a growth of a stiffener. In fact, *reduction can model the situation in which an intact, thin and finite-length material layer is present within a (uniformly) damaged material and progressively reduces its length, due to damage growth*.[2] This situation can be related to damage progression, which may under special circumstances spread through solids evidencing a fingering, similar in a sense to the fingering flow phenomena observable in porous systems or to the adhesion-induced instability in thin films (Saffman and Taylor, 1958; Ghatak and Chaudhury, 2003). Therefore, investigation of energy release rate for a stiffener change in length may shed light on the problem of damage growth in solids.

The incremental energy release rate for stiffener growth (we refer to growth to keep contact with the analogous problem of fracture mechanics, so that reduction is simply understood as a negative growth) is solved for incremental deformation superimposed upon a given state of stress and strain (initially assumed generic, but later uniform in the applications) of an incompressible elastic solid, such as that introduced in Part I of this article (in Section 3). However, since these results are new, we remark that the small strain theory and the compressible prestressed elasticity can be immediately obtained from our formulation.

It will be shown that, differently from the well-known formulae of fracture mechanics, the incremental energy release rate is always negative (so that reduction is always predicted and growth never occurs). Moreover, the incremental energy release rate is shown to vanish when the Elliptic boundary is approached (more precisely, there may be exceptions to this rule at the EI/P boundary, a circumstance that will be detailed later). This finding implies that the reduction of the stiffener dies out when the boundary of Ellipticity is approached and, at the same time, our previous results show that shear bands begin to emerge at the stiffener tip. We therefore find an intriguing interplaying between shear band nucleation and slowing down of stiffener reduction process.

## 2. Shear band nucleation and growth at the stiffener tip

The analytical solution found in Part I of this article (for a stiffener of length $2l$ embedded in an infinite elastic incompressible, orthotropic and uniformly prestressed medium, subject to a remote symmetric perturbation) is now employed to investigate the incremental fields until near the boundary of ellipticity loss.

All cases have been investigated for simplicity with a horizontal tensile or compressive prestress $\sigma_1$, while vertical prestress has been taken null, $\sigma_2 = 0$, so that $k = \eta$.

We begin with the simple case of a Mooney–Rivlin material, which is made orthotropic only by the presence of the prestress, so that the two incremental moduli remain constant, $\xi = 1$ (see Bigoni and Capuani, 2002, 2005 for a detailed explanation of the material models used throughout this section). Results are presented in Figs. 3 and 4, where the level sets are reported of the squared modulus of incremental deviatoric strain $|\mathrm{dev}\,\dot{\boldsymbol{\varepsilon}}|^2$

[2]In a different setting, stiffener and matrix could be the two (the former much stiff than the latter) phases of a material, so that stiffener growth or reduction would be related to a progression or regression of a phase transformation.

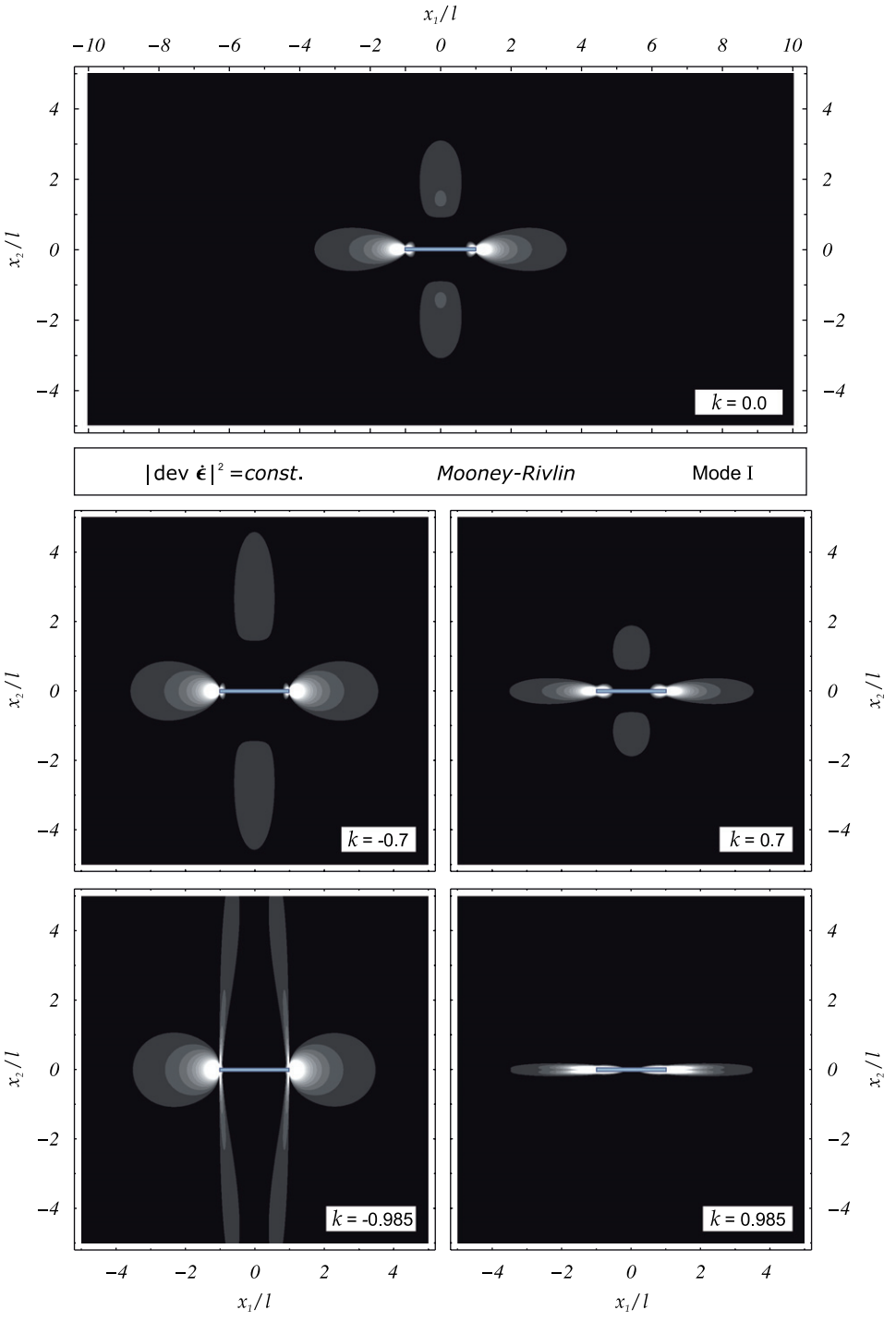


Fig. 3. Level sets of the second invariant of deviatoric incremental strain, $|\mathrm{dev}\,\dot{\boldsymbol{\varepsilon}}|^2$, near a stiffener of length $2l$ embedded in a Mooney–Rivlin material at different values of prestress parameter $k$ (increasing from the top to the bottom of the figure), under a Mode I perturbation. For $k = 0.985$ a shear band emerges aligned parallel to the stiffener, while for $k = -0.985$ two shear bands form orthogonally to the tips of the stiffener.

and displacement $|\mathbf{v}|$, for different values of the prestress dimensionless parameter $k$ [the grey scale is such that black (white) corresponds $|\mathrm{dev}\,\dot{\boldsymbol{\varepsilon}}|^2 \leqslant |\mathrm{dev}\,\dot{\boldsymbol{\varepsilon}}^{\infty}|^2$ ($|\mathrm{dev}\,\dot{\boldsymbol{\varepsilon}}|^2 \geqslant 2|\mathrm{dev}\,\dot{\boldsymbol{\varepsilon}}^{\infty}|^2$)]. According to the Mooney–Rivlin material model, the response always lies in the EI regime and reaches the EI/P boundary at an infinite stretch.

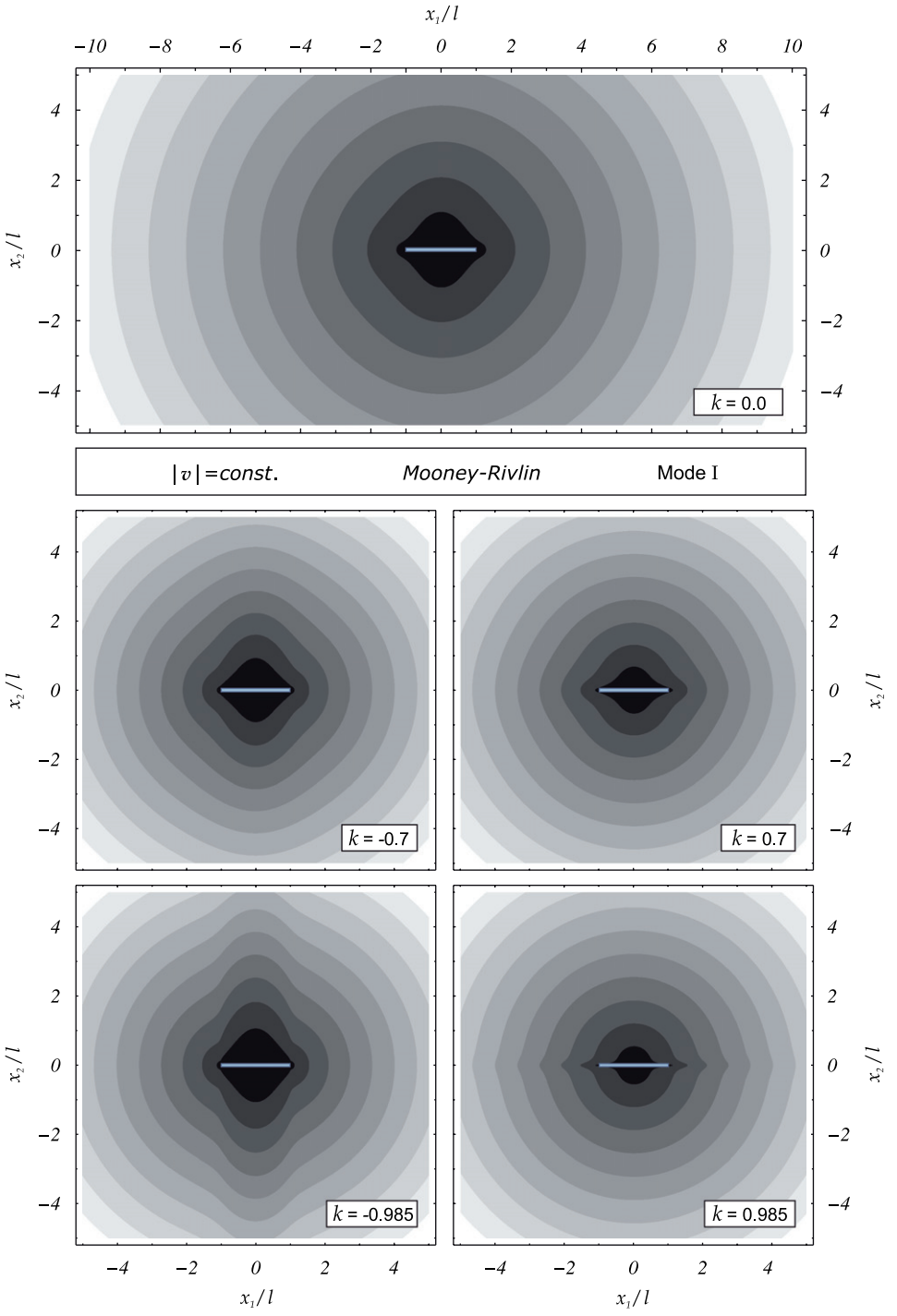


Fig. 4. Level sets of the modulus of incremental displacements $|\mathbf{v}|$, near a stiffener of length $2l$ embedded in a Mooney–Rivlin material at different values of prestress parameter $k$, under a Mode I perturbation.

Would this boundary be attained, a shear band in terms of discontinuity of velocity gradient across a planar band would be predicted to occur aligned parallel to the maximum prestress (which can be positive or null for uniaxial tension and compression, respectively).

The figures are organized as follows. The case of null prestress $k=0$ is on the upper part, while (the absolute value of) prestress increases from the top to the bottom of the figures, in particular $k=\pm 0.7$ and $\pm 0.985$ are considered. When the prestress is increased almost close to the boundary of ellipticity loss (which corresponds to $k=\pm 1$), shear bands clearly emerge. In particular, two shear bands form aligned parallel (or orthogonal) to the stiffener for tensile $k=0.985$ (or compressive, $k=-0.985$) prestress. The orthogonal bands nucleate as induced by a sort of 'Poisson effect'. As already noticed by Bigoni and Capuani (2002, 2005), even in the present context we find that shear bands, which are excluded in terms of incremental displacement gradient discontinuity for a Mooney–Rivlin material, become visible, thanks to our perturbative approach, in which the stiffener plays the role of a perturbing agent.

Results reported in Figs. 5–7 refer to a $J_2$-deformation theory material [the grey scale is such that black (white) corresponds $|\mathrm{dev}\,\dot{\boldsymbol{\varepsilon}}|^2 \leqslant |\mathrm{dev}\,\dot{\boldsymbol{\varepsilon}}^{\infty}|^2$ ($|\mathrm{dev}\,\dot{\boldsymbol{\varepsilon}}|^2 \geqslant 2.5|\mathrm{dev}\,\dot{\boldsymbol{\varepsilon}}^{\infty}|^2$)]. Here the prestrain is prescribed, in terms of the logarithmic strain $\varepsilon=\ln\lambda$ (where $\lambda$ is the in-plane maximum stretch). This parameter is used to 'tune' the distance to the Elliptic boundary, in particular, EC/H is now approached. The critical level of $\varepsilon$ for shear band formation in terms of incremental displacement gradient discontinuities and their inclination at the EC/H boundary can be calculated employing well-known formulae (see for instance Radi et al., 2002). In particular, $\varepsilon \simeq \pm 0.3216$ and $\pm 0.6778$ correspond to points at the EC/H boundary for the two values of the hardening parameter $N$, 0.1 and 0.4, assumed in the subsequent examples. The following shear band inclinations $\vartheta_0$ (measured from the $x_1$-axis, see Radi et al., 2002, their Fig. 9) can be calculated at the EC/H boundary:

- for $N=0.1$, $\vartheta_0 \simeq 35.942$ if $\varepsilon>0$ and $\vartheta_0 \simeq 54.058$ if $\varepsilon<0$;
- for $N=0.4$, $\vartheta_0 \simeq 26.918$ if $\varepsilon>0$ and $\vartheta_0 \simeq 63.082$ if $\varepsilon<0$.

Maps of the squared modulus of deviatoric incremental strain are reported in Figs. 5 and 6 for $N=0.1$ and 0.4, respectively, while maps of the modulus of incremental displacements are reported in Fig. 7, relative to $N=0.4$ (the case $N=0.1$ is almost identical and has not been reported for conciseness).

The striking difference between the Mooney–Rivlin case, Figs. 3–4, and the $J_2$-deformation theory of plasticity is the inclination of the shear bands, which, in the latter case, is similar to that typical of metals.

We end our investigation, reporting asymptotic results for Mode II loading in Figs. 8–12. In particular Figs. 8 and 9 pertain to a Mooney–Rivlin material, while Figs. 10–12 to a $J_2$-deformation theory material, both investigated at increasing values of prestress (for Mooney–Rivlin) or prestrain (for $J_2$-material).

As final comments, we remark that:

- the presence of a stiffener strongly promotes shear band formation;
- shear bands develop radially from the stiffener tip;
- shear bands maintain the inclination that can be calculated in terms of singularity of the acoustic tensor at the boundary of Ellipticity;
- the band inclination is independent of the perturbation mode.

## 3. Rigid inclusion growth (or reduction)

We attack now the problem of incremental energy release rate for stiffener growth. To this purpose, we refer to Fig. 13, where two incremental boundary value problems are compared (for finite bodies subject to identical conditions on the external boundaries $S_\sigma \cup S_v$, namely, prescribed incremental nominal tractions $\dot{\boldsymbol{\sigma}}^0$ on $S_\sigma$ and incremental displacements $\mathbf{v}=\bar{\mathbf{v}}$ on $S_v$; note the similarity with the void problem, see Rice, 1968, p. 205) only differing in the sizes of the rigid body that they contain. In particular, the inclusion in the body on the right (of volume $V_i \cup \Delta V_i$, enclosed by surface $S_i^* \cup \Delta S_i^*$) has been obtained by increasing the size of the inclusion in the body on the left (of volume $V_i$, enclosed by

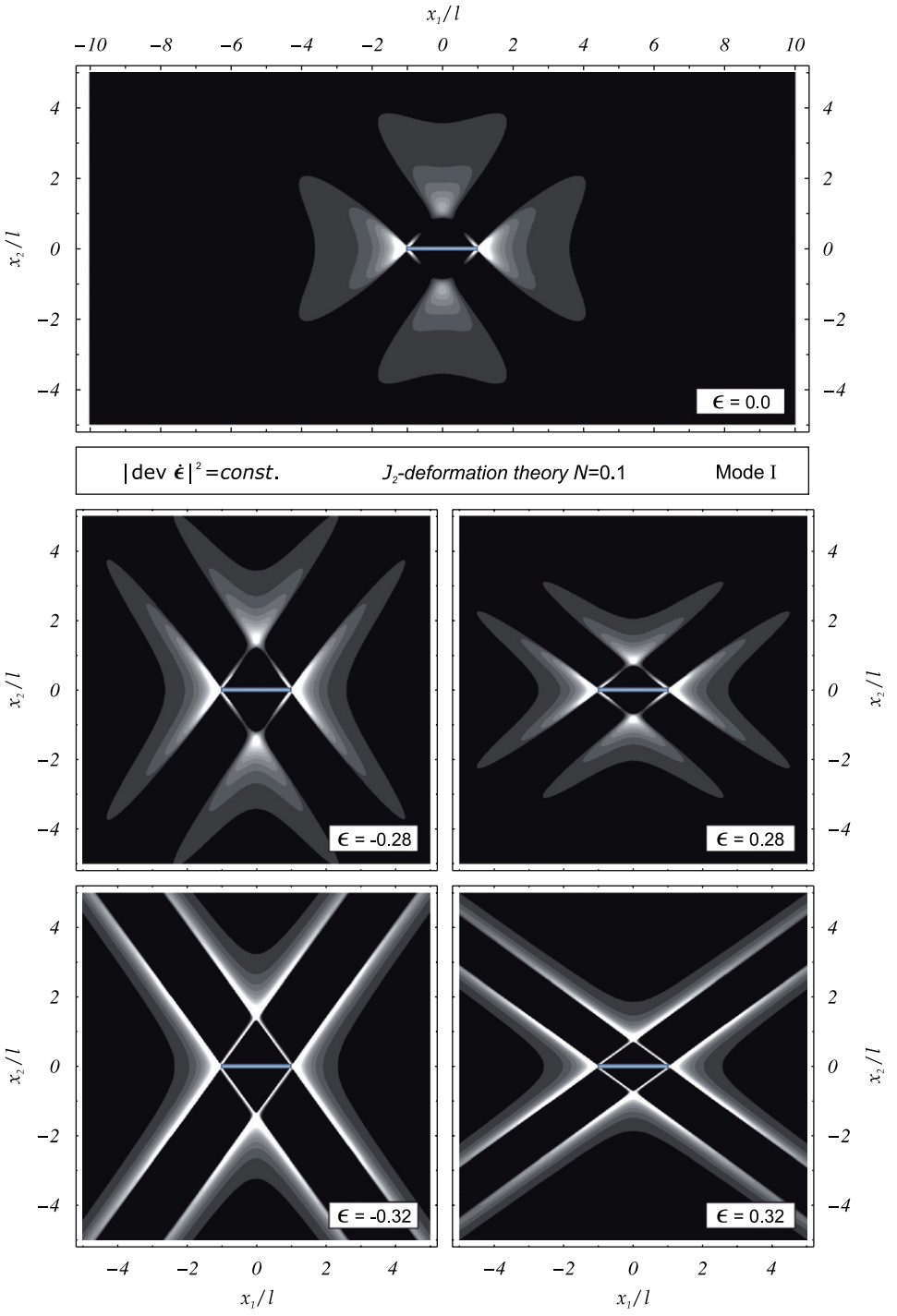


Fig. 5. Level sets of the second invariant of deviatoric incremental strain, $|\mathrm{dev}\,\dot{\boldsymbol{\varepsilon}}|^2$, near a stiffener of length $2l$ embedded in a $J_2$-deformation theory material with $N = 0.1$ at different values of logarithmic prestrain $\varepsilon$ (increasing from the top to the bottom of the figure), under a Mode I perturbation. For $\varepsilon = \pm 0.32$ shear bands emerge inclined to the stiffener. The inclination differs between tensile and compressive prestrain.

surface $S_i$). We define the incremental displacement and nominal traction fields, solutions to the two problems, as $\mathbf{v}^0$ and $\dot{\mathbf{t}}^0$ for the problem on the left and $\mathbf{v} = \mathbf{v}^0 + \tilde{\mathbf{v}}$ and $\dot{\mathbf{t}} = \dot{\mathbf{t}}^0 + \tilde{\mathbf{t}}$ for the problem on the right. Note that $\mathbf{v}^0$ and $\mathbf{v}$ are rigid body incremental displacements within $V_i$ and $V_i \cup \Delta V_i$, respectively.

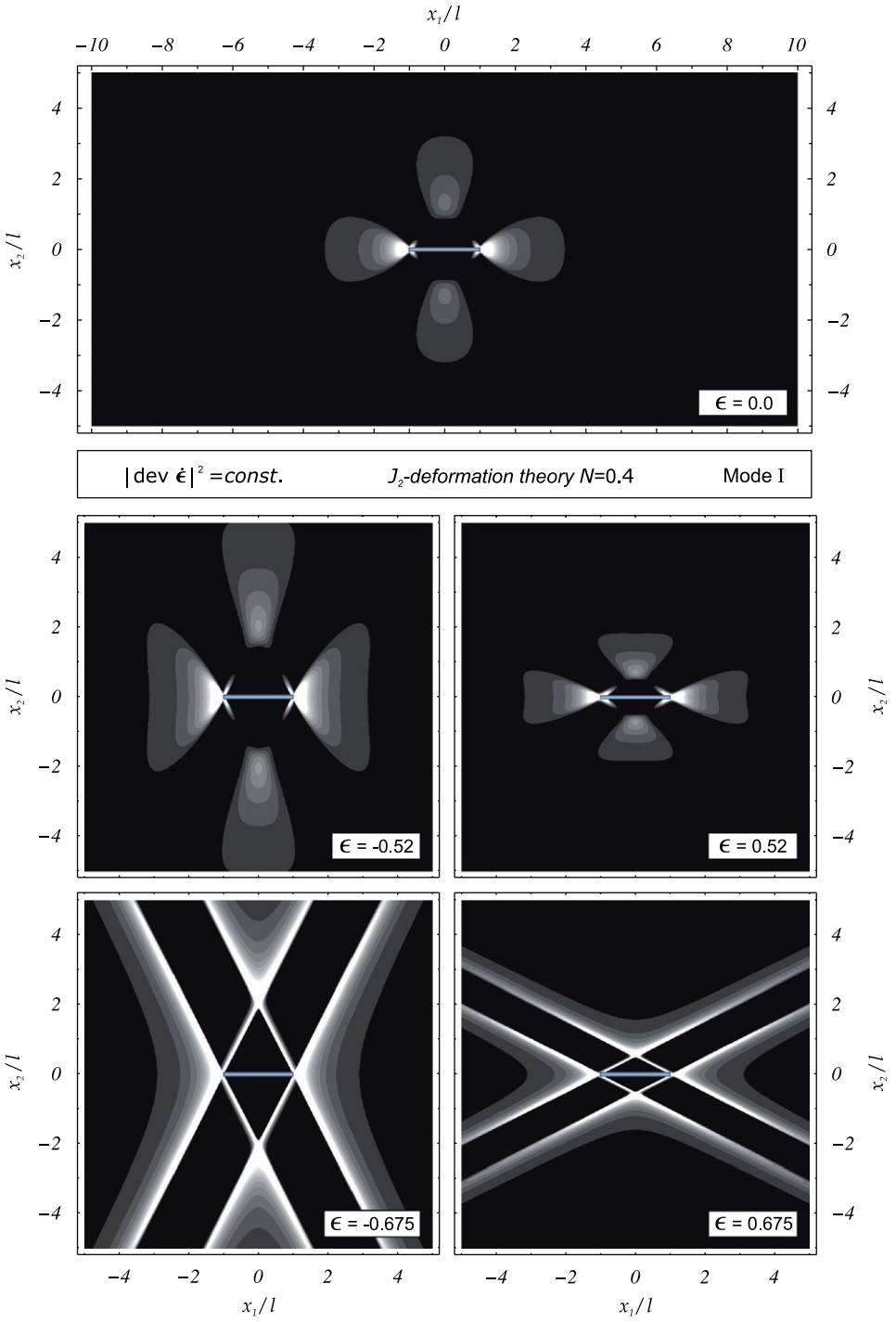


Fig. 6. As for Fig. 5, but for higher hardening exponent $N = 0.4$. Note the difference with the shear band inclinations visible in that figure.

The two bodies are assumed to be identically prestressed and prestrained, although not necessarily in a homogeneous way. Obviously, in order to have identical prestress and prestrain, the two current configurations shown in Fig. 13 cannot be reached through a continuous deformation path starting from unloaded configurations containing different rigid inclusions. The situation sketched in Fig. 13 can be

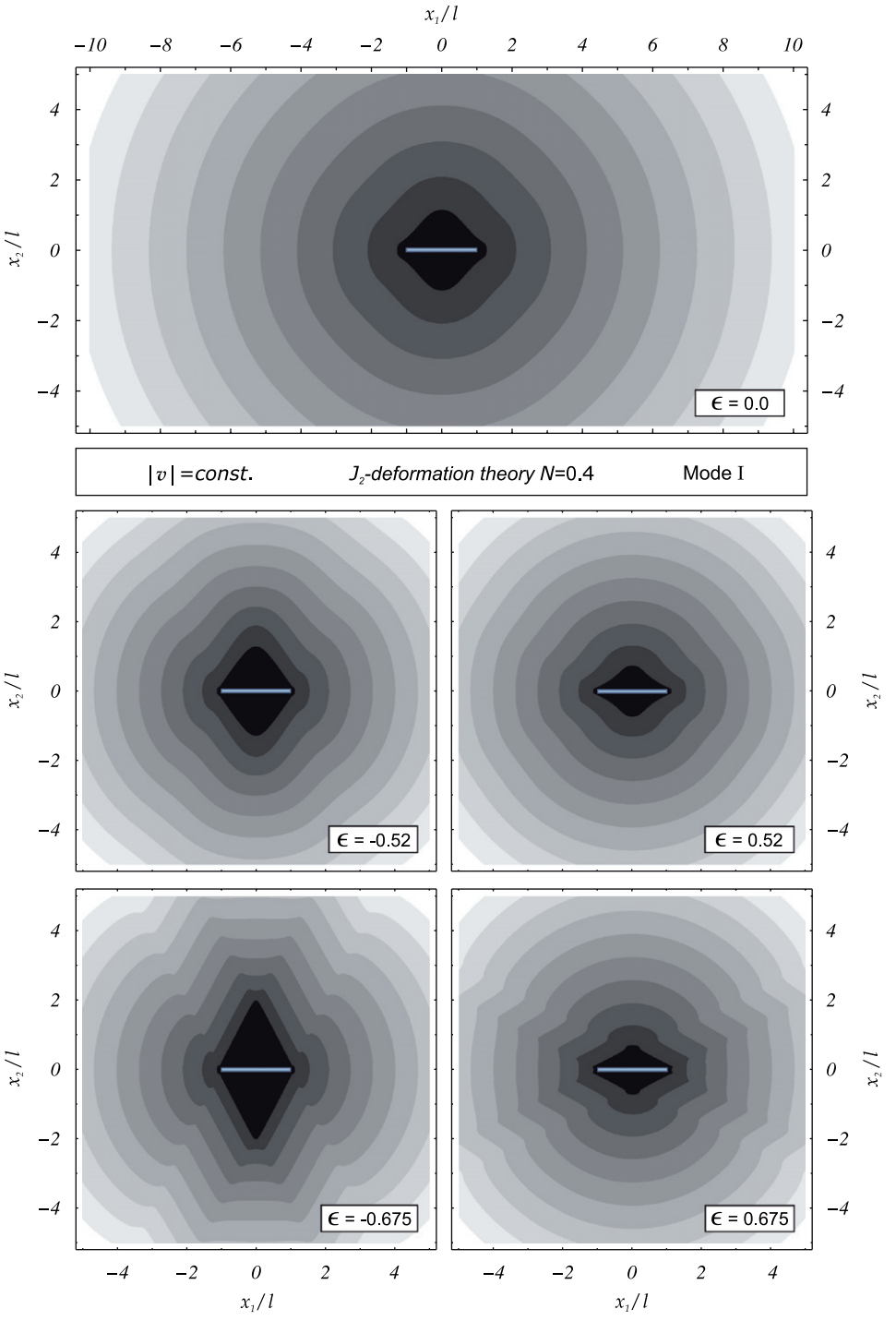


Fig. 7. Level sets of the modulus of incremental displacements $|\mathbf{v}|$, near a stiffener of length $2l$ embedded in a $J_2$-deformation theory material with $N = 0.4$ at different values of logarithmic prestrain $\varepsilon$, under a Mode I perturbation.

obtained through a 'rigidification' of different volumes (corresponding to the two inclusions) at a stage of a deformation process.[3]

[3]The rigidification could for instance be obtained in a porous material through infiltration of a resin.

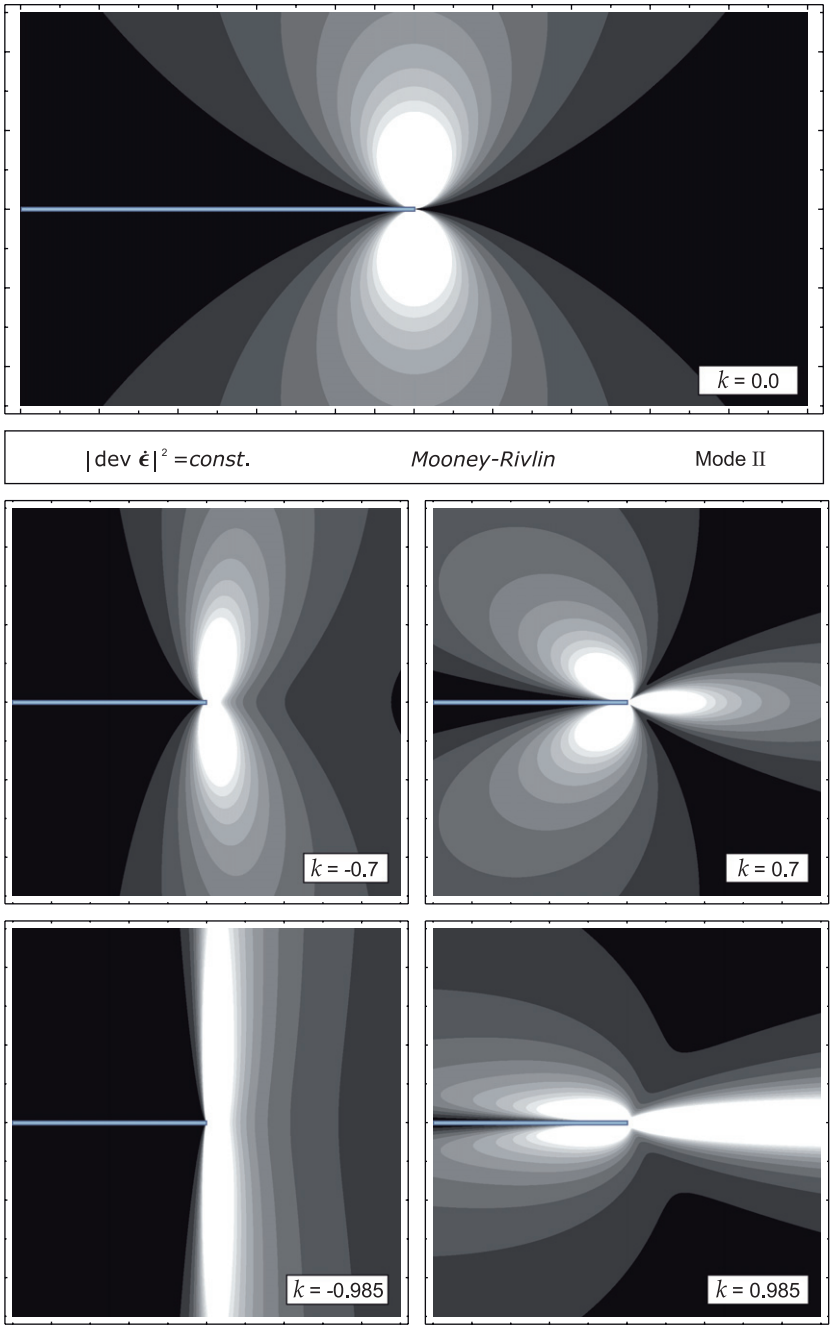


Fig. 8. Level sets of the second invariant of deviatoric incremental strain, $|\mathrm{dev}\,\dot{\boldsymbol{e}}|^2$, near the tip of a stiffener (asymptotic solution) embedded in a Mooney–Rivlin material at different values of prestress parameter $k$ (increasing from the top to the bottom of the figure), under a Mode II perturbation.

Neglecting body forces, the incremental potential energy functional $\dot{P}$ used by Hill (1961), minimal for the incremental displacement field solution of the incremental problem is

$$\dot{P}^0 = \int_V \phi(\nabla \mathbf{v}^0)\,\mathrm{d}V - \int_{S_\sigma} \dot{\boldsymbol{\sigma}}^0 \cdot \mathbf{v}^0\,\mathrm{d}S, \tag{1}$$

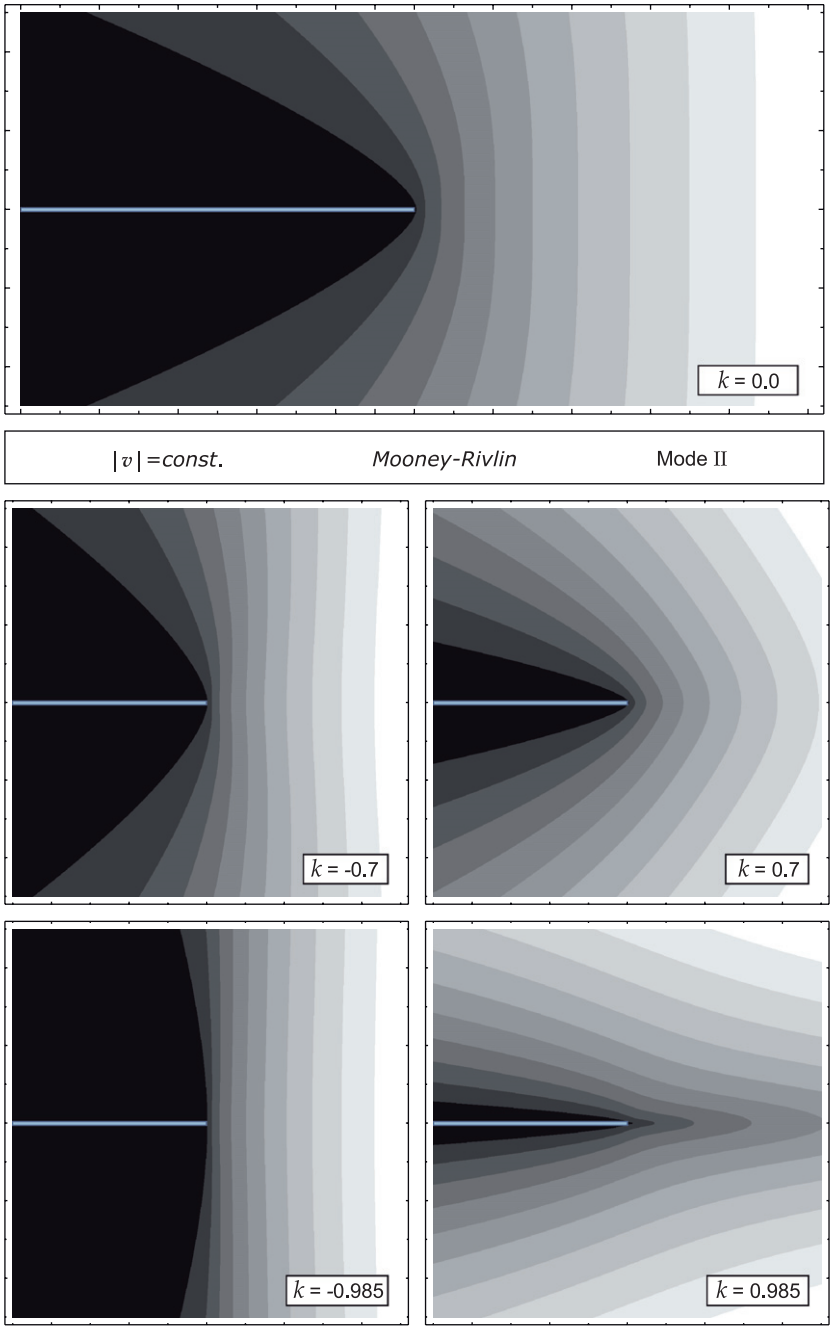


Fig. 9. Level sets of the modulus of incremental displacements $|\mathbf{v}|$, near the tip of a stiffener (asymptotic solution) embedded in a Mooney–Rivlin material at different values of prestress parameter $k$, under a Mode II perturbation.

for the body on the left in Fig. 13, and

$$\dot{P}^0 + \Delta\dot{P} = \int_{V\setminus\Delta V_i} \phi(\nabla\mathbf{v}^0 + \nabla\tilde{\mathbf{v}})\,\mathrm{d}V - \int_{S_\sigma} \dot{\boldsymbol{\sigma}}^0\cdot(\mathbf{v}^0 + \tilde{\mathbf{v}})\,\mathrm{d}S, \tag{2}$$

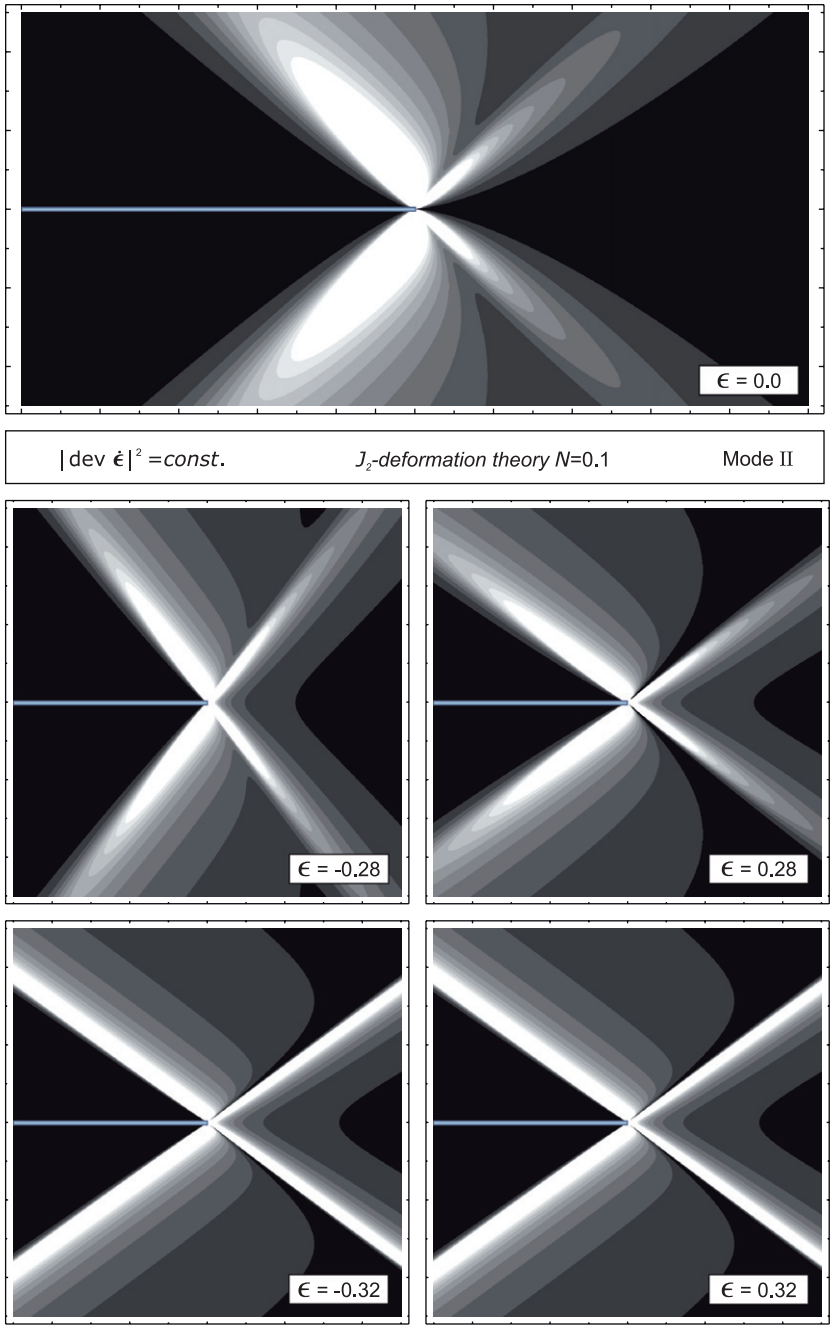


Fig. 10. Level sets of the second invariant of deviatoric incremental strain, $|\mathrm{dev}\,\dot{\boldsymbol{\varepsilon}}|^2$, near the tip of a stiffener (asymptotic solution) embedded in a $J_2$-deformation theory material with $N = 0.1$ at different values of logarithmic prestrain $\varepsilon$ (increasing from the top to the bottom of the figure), under a Mode II perturbation.

for the body on the right. The scalar function $\phi$ is the incremental displacement gradient potential defined as

$$\dot{t}_{ij} = \frac{\partial \phi(\nabla \mathbf{v})}{\partial v_{j,i}} + \dot{p}\,\delta_{ij}, \tag{3}$$

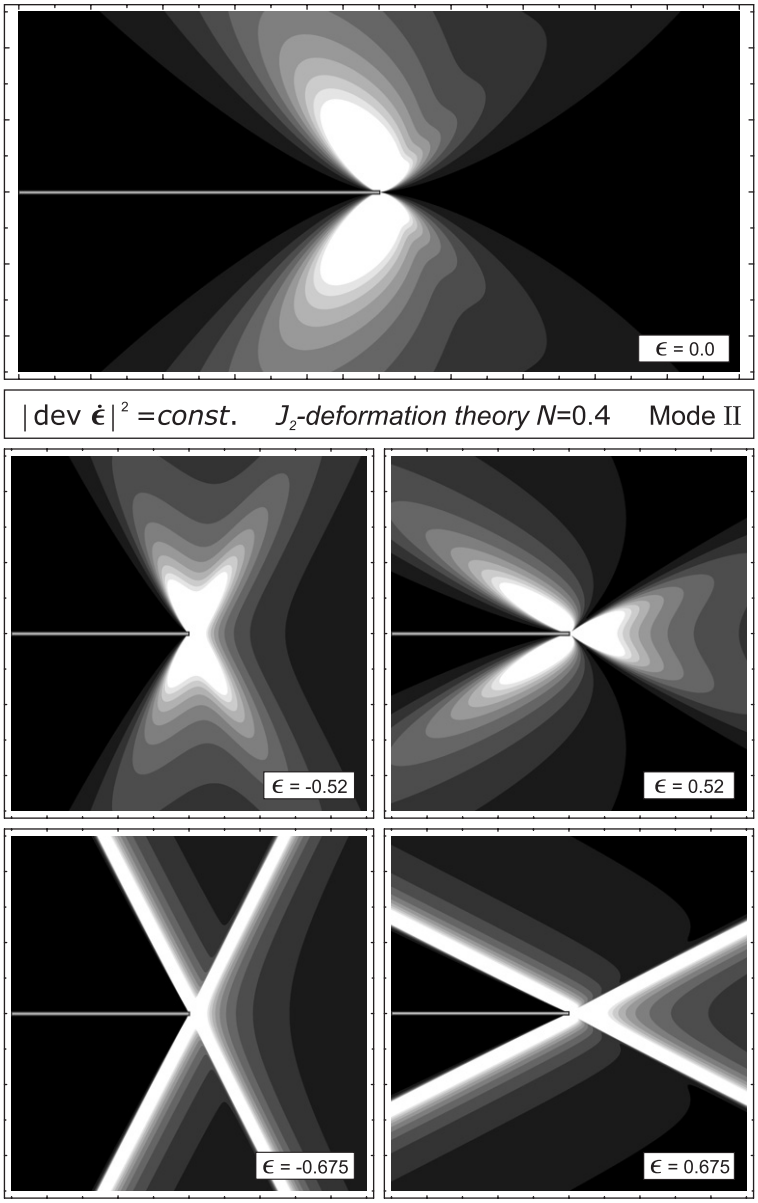


Fig. 11. As for Fig. 10, but for higher hardening exponent $N = 0.4$.

where $\dot{p}$ is the incremental, mean stress and $\delta_{ij}$ the Kronecker delta. Due to the linearity of the incremental solution, we can introduce the constitutive fourth-order tensor $\mathbb{K}$, so that

$$\phi(\nabla \mathbf{v}) = \tfrac{1}{2} v_{j,i} \mathbb{K}_{ijhk} v_{k,h}. \tag{4}$$

Note that when quantity $-\Delta\dot{P}$ is greater (smaller) than zero in Eqs. (1) and (2), growth (reduction) of the inclusion is expected. This quantity can be obtained by subtracting Eq. (2) from Eq. (1) as

$$-\Delta\dot{P} = \int_{\Delta V_i} \phi(\nabla \mathbf{v}^0)\,\mathrm{d}V - \int_{V\setminus\Delta V_i} \phi(\nabla \tilde{\mathbf{v}})\,\mathrm{d}V - \int_{V\setminus\Delta V_i} \tilde{\mathbf{t}}^{\mathrm{T}} \cdot \nabla \mathbf{v}^0\,\mathrm{d}V + \int_{S_\sigma} \dot{\boldsymbol{\sigma}}^0 \cdot \tilde{\mathbf{v}}\,\mathrm{d}S, \tag{5}$$

where T denotes the transpose.

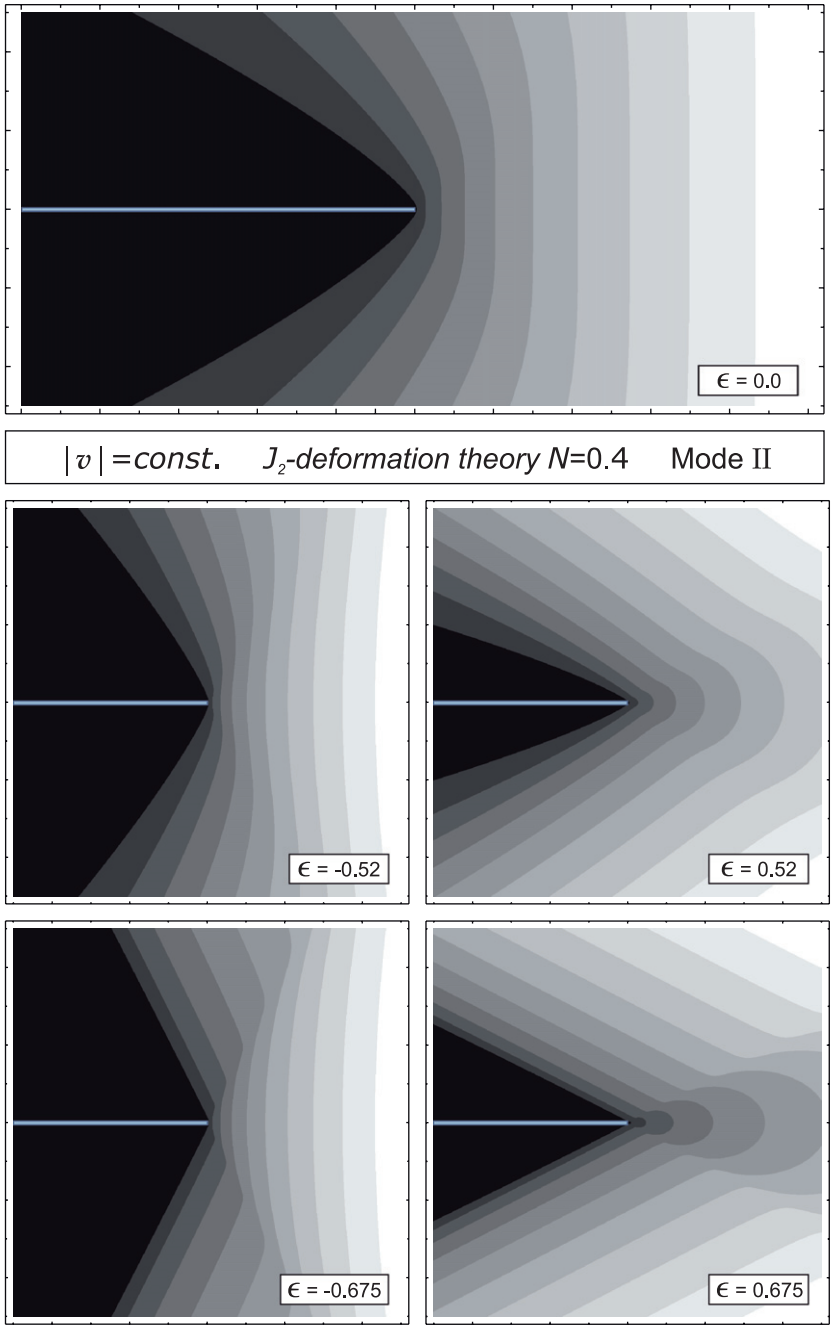


Fig. 12. Level sets of the modulus of incremental displacements $|\mathbf{v}|$, near the tip of a stiffener (asymptotic solution) embedded in a $J_2$-deformation theory material with $N = 0.4$ at different values of logarithmic prestrain $\varepsilon$, under a Mode II perturbation.

We begin noting that $\tilde{\mathbf{v}} = \mathbf{0}$ on $S_v$; moreover, we extend the nominal stress field $\dot{\mathbf{t}}$ inside the rigid inclusion (which is always possible using incremental equilibrium stress fields), therefore the divergence theorem applied to the domain on the left of Fig. 13 yields

$$\int_{S_\sigma} \dot{\boldsymbol{\sigma}}^0 \cdot \tilde{\mathbf{v}} \, \mathrm{d}S = \int_V \tilde{\mathbf{t}}^{\mathrm{T}} \cdot \nabla \mathbf{v}^0 \, \mathrm{d}V, \tag{6}$$

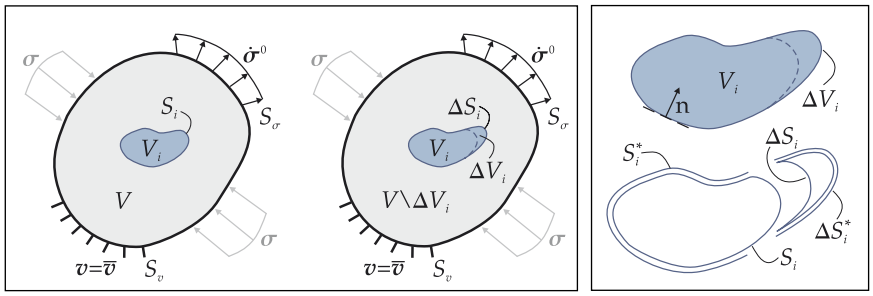


Fig. 13. Two elastic, prestressed bodies are compared (left), having identical shape, boundary conditions, elastic properties, prestress, and prestrain, but inclusions of different size. The detail of the rigid inclusion and its surface is reported on the right; note the unit normal vector, defined to point outward the elastic body and toward the inclusion.

where, as $\phi(\nabla\mathbf{v})$ in Eq. (4) is a biquadratic form, the equality

$$\mathbf{t}^{0\mathrm{T}}\cdot\nabla\tilde{\mathbf{v}} = \tilde{\mathbf{t}}^{\mathrm{T}}\cdot\nabla\mathbf{v}^0, \tag{7}$$

has been exploited. We therefore arrive at

$$-\Delta\dot{P} = \int_{\Delta V_i}\phi(\nabla\mathbf{v}^0)\,\mathrm{d}V - \int_{V\backslash\Delta V_i}\phi(\nabla\tilde{\mathbf{v}})\,\mathrm{d}V + \int_{\Delta V_i}\tilde{\mathbf{t}}^{\mathrm{T}}\cdot\nabla\mathbf{v}^0\,\mathrm{d}V. \tag{8}$$

Noting again that the field $\dot{\mathbf{t}}$ extended into the rigid inclusion makes the field $\tilde{\mathbf{t}}$ equilibrated at every point and that $\mathbf{v}^0$ is a rigid-body incremental displacement within the inclusion $V_i$, we have

$$\int_{\Delta V_i}\tilde{\mathbf{t}}^{\mathrm{T}}\cdot\nabla\mathbf{v}^0\,\mathrm{d}V = -2\int_{\Delta V_i}\phi(\nabla\mathbf{v}^0)\,\mathrm{d}V. \tag{9}$$

Since $\tilde{\boldsymbol{\sigma}} = \tilde{\mathbf{t}}^{\mathrm{T}}\mathbf{n} = \mathbf{0}$ on $S_\sigma$, application of the divergence theorem to the domain on the right of Fig. 13 provides

$$-\int_{V\backslash\Delta V_i}\phi(\nabla\tilde{\mathbf{v}})\,\mathrm{d}V = \frac{1}{2}\int_{S_i^*\cup\Delta S_i^*}\tilde{\mathbf{t}}^{\mathbf{T}}\mathbf{n}\cdot\mathbf{v}^0\,\mathrm{d}S, \tag{10}$$

obtaining finally

$$-\Delta\dot{P} = -\int_{\Delta V_i}\phi(\nabla\mathbf{v}^0)\,\mathrm{d}V + \frac{1}{2}\int_{S_i^*\cup\Delta S_i^*}\tilde{\mathbf{t}}^{\mathbf{T}}\mathbf{n}\cdot\mathbf{v}^0\,\mathrm{d}S. \tag{11}$$

Note that Eq. (11) is valid both for compressible and incompressible materials since $\dot{p}$ in Eq. (3) is workless.

*Eq.* (11) *represents the incremental potential energy decrease for a growth of a rigid inclusion in an elastic, incompressible or compressible body, generically anisotropic and prestressed. It is transparent from Eqs.* (10) *and* (11), *that the incremental potential energy decrease is always negative, implying a reduction of the inclusion.*

Note that the second integral on the right-hand side of Eq. (11) is extended on the whole rigid inclusion (having an external surface $S_i^* \cup \Delta S_i^*$). To keep contact with the analogous void problem, it is expedient now to re-write Eq. (11) with reference to the surface $\Delta S_i$ enclosing the volume $\Delta V_i$, namely

$$-\Delta\dot{P} = -\int_{\Delta V_i}\phi(\nabla\mathbf{v}^0)\,\mathrm{d}V + \frac{1}{2}\int_{\Delta S_i}\tilde{\mathbf{t}}^{\mathbf{T}}\mathbf{n}\cdot\mathbf{v}^0\,\mathrm{d}S, \tag{12}$$

and split the incremental displacement field as

$$\mathbf{v}^0 = \mathbf{v}^* + \hat{\mathbf{v}}, \tag{13}$$

where $\mathbf{v}^*$ vanishes inside the rigid inclusion $V_i$ and $\hat{\mathbf{v}}$ is the rigid body incremental displacement of the inclusion extended to the whole body $V$. The incremental potential energy decrease is not affected by $\hat{\mathbf{v}}$, while, in the

second term of Eq. (12) the integral along $\Delta S_i \backslash \Delta S_i^*$ is null because $\mathbf{v}^*$ vanishes there. We therefore obtain

$$-\Delta\dot{P} = -\int_{\Delta V_i} \phi(\nabla \mathbf{v}^*)\,\mathrm{d}V + \frac{1}{2}\int_{\Delta S_i^*} \tilde{\mathbf{t}}^{\mathrm{T}}\mathbf{n}\cdot\mathbf{v}^*\,\mathrm{d}S. \tag{14}$$

*Eq.* (14) *represents the incremental potential energy decrease for a growth of a rigid inclusion in an elastic (incompressible or compressible, generically anisotropic and prestressed) body, expressed analogously to the corresponding expression in the void problem [see Rice, 1968, his Eq. (55), p. 207].*

### 3.1. A lamellar rigid inclusion

Turning now the attention to a thin rigid body, namely, a stiffener, the volume integral in Eq. (11) vanishes, so that taking the limit of the length increase $\Delta a \to 0$ at fixed incremental stress intensity factor $\dot{K}$, Eq. (14) becomes

$$\dot{G} = -\frac{\mathrm{d}\dot{P}}{\mathrm{d}a} = \lim_{\Delta a\to 0}\frac{1}{\Delta a}\int_0^{\Delta a} \dot{\mathbf{t}}^{\mathrm{T}}\mathbf{n}(\Delta a - r, \pi)\cdot\mathbf{v}(r, 0)\,\mathrm{d}r, \tag{15}$$

thus defining

*the incremental energy release rate for a growth of a stiffener in an elastic, incompressible or compressible body, generically anisotropic and prestressed.*

It can be easily verified that the incremental energy release rate coincides with the path-independent incremental $J$-integral

$$\dot{G} = \dot{J} = \int_\Gamma \left(\phi n_1 - \dot{\mathbf{t}}^{\mathrm{T}}\mathbf{n}\cdot\frac{\partial \mathbf{v}}{\partial x_1}\right)\mathrm{d}\Gamma. \tag{16}$$

#### 3.1.1. The incremental energy release rate for stiffener growth

The incremental energy release rate (15) can be written as

$$\dot{G}_{\mathrm{I}} = -\lim_{\Delta a\to 0}\frac{1}{\Delta a}\int_0^{\Delta a} \dot{t}_{21}(\Delta a - r, \pi)v_1(r, 0)\,\mathrm{d}r, \tag{17}$$

for Mode I loading and

$$\dot{G}_{\mathrm{II}} = -\lim_{\Delta a\to 0}\frac{1}{\Delta a}\int_0^{\Delta a} \dot{t}_{22}(\Delta a - r, \pi)v_2(r, 0)\,\mathrm{d}r, \tag{18}$$

for Mode II loading (note the differences with the analogous formulae for fracture mechanics, see Cristescu et al., 2004).

In the absence of prestress and for compressible isotropic elasticity, the available expression for energy release rate for stiffener growth (Wang et al., 1985) is not similar to that corresponding to fracture growth. Employing our definition of stress intensity factors, it becomes now possible to express the energy release rate for stiffener growth in a form strictly similar to that known for a fracture, which is obtained for the infinitesimal theory in Appendix A. That expression can be generalized for incremental deformations superimposed upon a given homogeneous state of stress using the asymptotic analysis derived in Part I of this paper as

$$\dot{G} = -\frac{\dot{K}^2_{(\varepsilon)\mathrm{I}}\sqrt{1-k} + \dot{K}^2_{(\varepsilon)\mathrm{II}}\sqrt{1+k}}{4\sqrt{2}\mu}\sqrt{2\xi - 1 + \sqrt{1-k^2}}, \tag{19}$$

valid in both the EI and EC regimes and independent of $\eta$. Note that the negative sign in Eq. (19) shows that

*reduction of the stiffener is always predicted.*

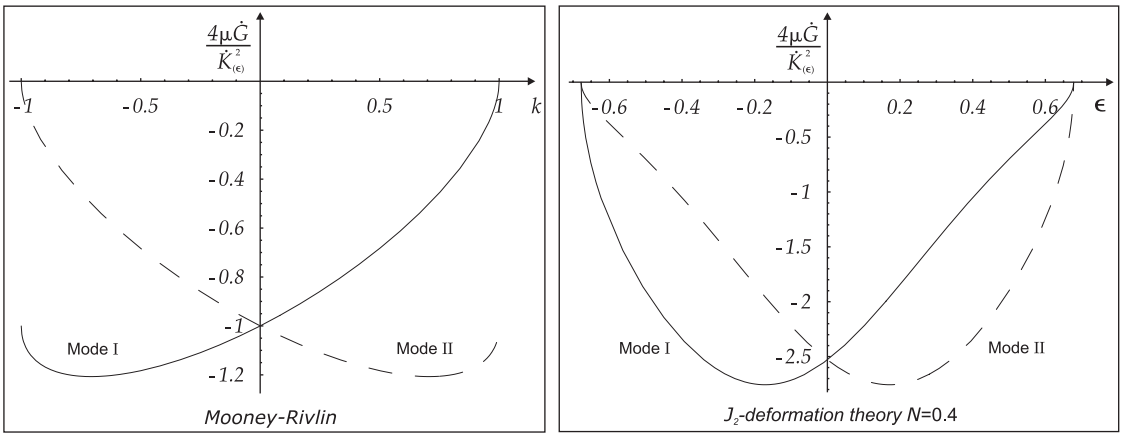


Fig. 14. Incremental energy release rate in a Mooney–Rivlin (left) and a $J_2$-deformation theory (right) material. Note that the incremental release rate always vanishes at the EC/H boundary, except for Mooney–Rivlin material at $k=-1$ for Mode I and $k=1$ for Mode II.

The incremental energy release rate (19) is represented in Fig. 14 for Mooney–Rivlin material (left) and $J_2$-deformation theory material (right) as a function of the prestress parameter $k$ in the former case and of the prestrain parameter $\varepsilon$ in the latter.

The most interesting feature emerging from Fig. 14 is that $\dot{G}$ always vanishes at the EC/H boundary, since here the following condition holds true:

$$2\xi - 1 + \sqrt{1-k^2} = 0. \tag{20}$$

At the EI/P boundary the situation is more complicated, so that $\dot{G}$ becomes null at $k=1$ and $k=-1$ for Modes I and II, respectively, but remains different from zero in the other cases. This conclusion can be reached solving Eq. (19) for $k=\pm 1$, which gives

$$\dot{G} = -\frac{\sqrt{2\xi-1}}{4\mu} \times \begin{cases} \dot{K}^2_{(\varepsilon)\mathrm{II}} & \text{for } k=1, \\ \dot{K}^2_{(\varepsilon)\mathrm{I}} & \text{for } k=-1. \end{cases} \tag{21}$$

Note that when the incremental energy release rate vanishes, reduction of the stiffener is inhibited.

To understand the reasons for the vanishing or not of the incremental energy release rate, it becomes instrumental to digress now on the evaluation of the incremental axial force along the stiffener. Since a full-field solution is needed and this has been found (in Part I of the present paper) for Mode I (since for Mode II the stiffener is neutral), the following analysis is restricted to this condition.

### 3.1.2. *The incremental axial force in the stiffener under Mode I perturbation*

In order to evaluate the incremental axial force in the stiffener, we note that the load symmetry implies that the stiffener is subject only to axial force $\dot{\mathcal{N}}(x_1)$, which can be computed by means of the nominal shear stress increment $\dot{t}_{21}$ as

$$\dot{\mathcal{N}}(x_1) = \int_{x_1}^{l} [\dot{t}_{21}(y,0^+) - \dot{t}_{21}(y,0^-)]\,\mathrm{d}y. \tag{22}$$

Using the expressions for the nominal shear stress increments obtained in Part I of the present article, we get

$$\dot{\mathcal{N}}(x_1) = -2\sqrt{2}\mu v^{(\infty)}_{2,2}\sqrt{1-k}\sqrt{2\xi-1+\sqrt{1-k^2}}\sqrt{l^2-x_1^2}, \tag{23}$$

valid in both the EI and EC regimes and independent of $\eta$.

Values of the incremental axial force in the stiffener $\dot{\mathcal{N}}$ (divided by $4\mu v^{(\infty)}_{1,1}$ so that a dilatation parallel to the stiffener is considered) are reported in Fig. 15 for Mooney–Rivlin material and $J_2$-deformation theory

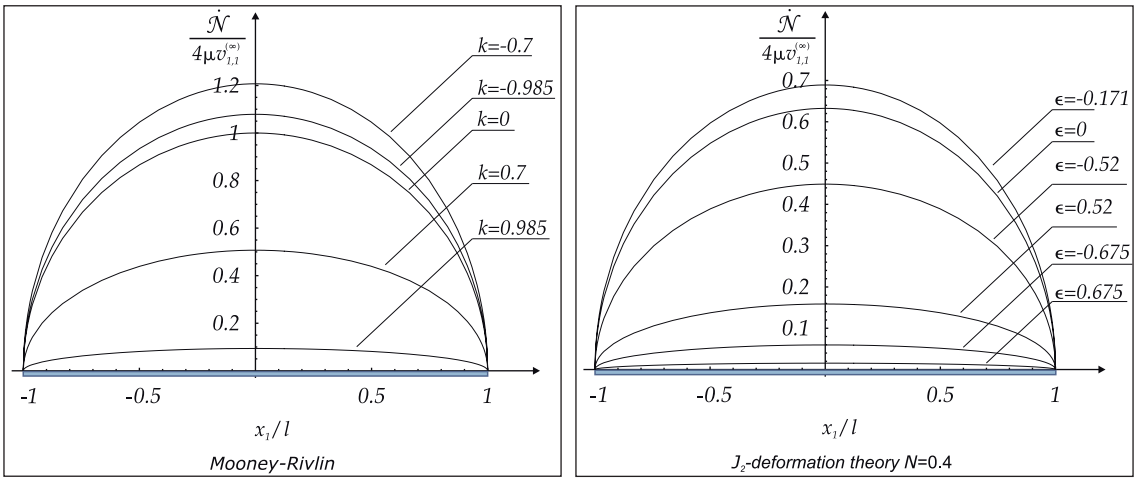


Fig. 15. The incremental axial force in a stiffener embedded in a prestressed Mooney–Rivlin material (left, for different values of prestress $k$) and in a $J_2$-deformation theory material (right, for different values of logarithmic prestrain $\varepsilon$). Note that the incremental axial force in the stiffener vanishes at the Elliptic boundary ($k = 1$ for Mooney–Rivlin and $\varepsilon = \pm 0.6778$ for $J_2$-deformation theory).

material, with $N = 0.4$, for different values of prestress in the former case and logarithmic prestrain in the latter.

It can be noted from Fig. 15 and, more precisely, from Eq. (23) that

- the maximum incremental axial force in the stiffener is always attained at $x_1 = 0$;
- the incremental axial force in the stiffener vanishes (i) always at the EC/H boundary, (ii) when $k = 1$ at the EI/P boundary. In other words, the incremental axial force does not vanish only at the EI/P boundary when $k = -1$.

The last of the above points can be explained considering that at the EI/P boundary, with $k = -1$, a shear band forms *orthogonally* to the stiffener tips, so that this can continue to carry an axial load.

Now we are in a position to set the relation (for a uniform Mode I loading) between the incremental energy release rate, $\dot{G}_{\mathrm{I}}$, and the maximum value of the incremental axial force in the stiffener

$$\dot{\mathcal{N}}_{\max} = \dot{\mathcal{N}}(x_1 = 0), \tag{24}$$

[where $\dot{\mathcal{N}}$ is given by Eq. (23)] which indeed can be obtained as

$$\dot{G}_{\mathrm{I}} = \frac{\pi v_{2,2}^{(\infty)}}{4} \dot{\mathcal{N}}_{\max}. \tag{25}$$

Eq. (25) explains the fact that the incremental Mode I energy release rate vanishes if and only if the incremental maximum axial force vanishes too, a circumstance clarifying the conditions for annihilation or not of stiffener reduction.

## 4. Conclusions

Shear bands have been found to emanate from the tips of a stiffener embedded in an infinite, uniformly prestressed elastic medium, as the response to Mode I or II perturbations, when prestress approaches the Elliptic boundary. The growth of these shear bands is shown to occur radially and with the inclination that can be calculated at the boundary of Ellipticity (using the well-known procedure based on the acoustic tensor singularity). For a solid approaching the Elliptic Imaginary/Parabolic boundary (as for instance a Mooney–Rivlin material), the shear bands may be aligned parallel or orthogonal to the stiffener, while

shear bands always result inclined, when the Elliptic Complex/Hyperbolic boundary (as for $J_2$-deformation theory material) is approached.

The problem of energy release rate connected with stiffener change in length (which may be of interest to attack problems such as damage diffusion or phase transformations in solids) has been addressed and solved, for the first time, under general assumptions. This result has been used to show that (i) a stiffener always reduces its length, (ii) the axial force carried by a stiffener usually vanishes at the Elliptic boundary, and (iii) in this circumstance stiffener reduction is inhibited.

## Acknowledgment

Financial support of MIUR-PRIN 2005 (prot. 2005085973) is gratefully acknowledged.

## Appendix A. Energy release rate for a stiffener embedded in a linear, compressible and isotropic elastic material

We begin noting that, similarly to the incompressible case reported in Part I of this article, the recourse to the following definition of stress intensity factors becomes instrumental also for compressible small strain elasticity:

$$K_{(\varepsilon)\mathrm{I}} = \lim_{r\to 0} 2\mu\sqrt{\kappa}\sqrt{2\pi r}\, u_{2,2}(r, \vartheta = 0),$$

$$K_{(\varepsilon)\mathrm{II}} = \lim_{r\to 0} 2\mu\sqrt{\kappa}\sqrt{2\pi r}\, u_{2,1}(r, \vartheta = 0), \tag{A.1}$$

where $u_i$ $(i = 1,2)$ is the displacement and $\kappa = 3 - 4\nu$ for plane strain, while $\kappa = (3 - \nu)/(1 + \nu)$ for plane stress. Definitions (A.1) coincide with the corresponding equations used in Part I when $\nu = 0.5$ in plane strain.

Employing the definition (A.1), the energy release rate for stiffener growth can be obtained from the asymptotic formula expressing the near-tip fields in the form

$$G = -(1 + \kappa)\frac{K^2_{(\varepsilon)\mathrm{I}} + K^2_{(\varepsilon)\mathrm{II}}}{8\mu}, \tag{A.2}$$

which, except for the negative sign (implying stiffener reduction), has the same expression for energy release rate in the crack growth problem.

In the incompressible limit and plane strain, the energy release rate (A.2) can be expressed as

$$G = -\frac{K^2_{(\varepsilon)\mathrm{I}} + K^2_{(\varepsilon)\mathrm{II}}}{4\mu}, \tag{A.3}$$

which can alternatively be (directly) obtained setting $k = 0$ and $\xi = 1$ in Eq. (19).

## References

Bigoni, D., Capuani, D., 2002. Green's function for incremental, nonlinear elasticity: shear bands and boundary integral formulation. J. Mech. Phys. Solids 50, 471–500.

Bigoni, D., Capuani, D., 2005. Time-harmonic Green's function and boundary integral formulation for incremental nonlinear elasticity: dynamics of wave patterns and shear bands. J. Mech. Phys. Solids 53, 1163–1187.

Cristescu, N.D., Craciun, E.M., Soós, E., 2004. Mechanics of Elastic Composites. Chapman & Hall/CRC, Boca Raton, FL.

Ghatak, A., Chaudhury, M.K., 2003. Adhesion-induced instability patterns in thin confined elastic film. Langmuir 19, 2621–2631.

Hill, R., 1961. Bifurcation and uniqueness in non-linear mechanics of continua. In: Lavrent'ev M.A., et al. (Eds.), Problems of Continuum Mechanics, SIAM, Philadelphia, PA, pp. 155–164.

Öztürk, T., Poole, W.J., Embury, J.D., 1991. The deformation of Cu-W laminates. Mater. Sci. Eng. A 148, 175–178.

Radi, E., Bigoni, D., Capuani, D., 2002. Effects of pre-stress on crack-tip fields in elastic, incompressible solids. Int. J. Solids Struct. 39, 3971–3996.

Rice, J.R., 1968. Mathematical analysis in the mechanics of fracture. In: H. Liebowitz (Ed.), Fracture, vol. II, Academic Press, New York, pp. 191–311.

Saffman, P.G., Taylor, G.I., 1958. The penetration of a fluid into a porous medium or Hele-Shaw cell containing a more viscous liquid. Proc. R. Soc. Lond. A 245, 312–329.

Wang, Z.Y., Zhang, H.T., Chou, Y.T., 1985. Characteristics of the elastic field of a rigid line inhomogeneity. J. Appl. Mech. 52, 818–822.